Time series analysis based study of a mass-spring-like oscillation and detachment of a metal pendant droplet

Andrej Jeromen[a,*] and Edvard Govekar[a]

[a] *University of Ljubljana, Faculty of Mechanical Engineering, Aškerčeva 6, 1000 Ljubljana, Slovenia*

* Corresponding author. Tel. +386 1 4771514, Fax +386 1 2518567, E-mail: andrej.jeromen@fs.uni-lj.si.

Link to published article:
http://www.sciencedirect.com/science/article/pii/S0888327016300772

DOI: 10.1016/j.ymssp.2016.04.038

Abstract

The subject of this study is the vertical mass-spring-like oscillation of a pendant droplet and its resonant detachment, which was experimentally observed in the process of laser droplet generation from a metal wire. The process was characterized by various time series, which were generated from a sequence of infrared intensity images of the process. Following a visual inspection of pendant droplet images and an analysis of a wavelet based time-frequency map of the droplet's vertical displacement time series, the pendant droplet's oscillation is described by a time-variable mass-spring system. Based on the characteristics of the time-frequency map, the resonant nature of the pendant droplet detachment was demonstrated. Additionally, an algebraic expression was formulated, which can be used to predict the detached droplet's diameter as a function of the laser pulse frequency.

Keywords: time series; time-frequency analysis; pendant droplet; mass-spring system; droplet detachment

1. Introduction

In recent years, metal droplets have been used in many innovative technologies, such as the joining of electrical contacts [1-3], and 3D structuring [4]. Among various methods for metal droplet generation, which form a basis for the above technologies, laser droplet generation (LDG) from a wire [5, 6] has been developed. In the LDG from a wire process, a laser beam is used to melt the end of the metal wire which is fed into the laser beam focus. Under the action of gravity and surface tension forces, a pendant droplet is formed from the molten wire-end and detached from the wire-end.

LDG is a complex process since it involves many physical phenomena such as light-matter interaction, heat diffusion, phase transitions, surface tension, and fluid flow. In the case of the generation of droplets in a sequence, the complexity of the LDG process increases further. The sequence of droplets can be generated either as a discrete drop-on-demand sequence [6] or as a continuous droplet sequence [5]. In both cases, the pendant droplet detachment is the most crucial phase since it affects the dynamics of the droplet sequence generation as well as the properties of the detached droplets.

Since a comprehensive theoretical study of such a complex process would be overly difficult, the LDG process has been mainly studied experimentally based on the analysis of various time series, such as acoustic emission [7], the intensity of reflected laser light [8], and high-speed infrared (IR) sensitive camera image sequences [5, 9]. Based on nonlinear analysis of time series generated from the IR image sequences, it has been shown that the process of laser droplet sequence generation, consisting of repeated drop-on-demand LDG, is in fact a low-dimensional chaos [9, 10] and, as such, very sensitive to the initial conditions. It has also been shown that the dynamics of the observed marginal detachment regimes, i.e. spontaneous dripping and forced detachment, are chaotic, with an intermittent transition between them [11].

As an alternative to the discrete drop-on-demand sequence generation process, a continuous LDG process has recently been realized by constant feeding of a metal wire into the focus of the pulsed laser beam which is used to melt the wire [5]. Based on the recorded IR image sequences, four different detachment mechanisms were experimentally observed in different laser pulse frequency ranges. Particularly, in the laser pulse frequency range between 60 Hz and 190 Hz, a distinct vertical oscillation of the pendant droplet, resembling a mass-spring system oscillation, was observed to lead to detachment of the pendant droplet. It was also observed experimentally that the above described detachment regime can lead to very regular droplet generation regarding the detachment frequency, the detached droplet diameter, and its lateral scatter [5]. As such, the continuous LDG process, and in particular the observed mass-spring oscillation and the related pendant droplet detachment, is a potential candidate for engineering applications. For this reason, if the properties of the detached droplet need to be predicted, then a deeper insight into the LDG process dynamics and the corresponding droplet detachment mechanism is needed.

In this paper, a time series analysis based study of the mass-spring-like pendant droplet vertical oscillation and its detachment in the continuous LDG process at laser pulse frequencies between 60 Hz and 190 Hz is presented. The study was based on the analysis of various time series, which were generated from the recorded IR intensity images of the process. The goal of the study was to gain an insight into the observed process dynamics, and in particular to determine the parameters of a simplified, low-dimensional, time-variable mass-spring model of the pendant droplet oscillations as well as to identify the mechanism of pendant droplet detachment, which occurred in the laser pulse frequency range between 60 Hz

and 190 Hz. With this aim, in the following section the experimental setup for the LDG, the experiments, and the data resulting from the experiments, are presented. In third section, the generation of the time series that were used for the analysis is described. The fourth section presents the time-frequency based analysis of the generated time series, which resulted in a description of the pendant droplet as a forced time-variable mass-spring system and the determination of related system parameters. Additionally, the resonant nature of the pendant droplet detachment was shown. Finally, based on the preceding analysis, an algebraic expression for the prediction of the detached droplet diameter depending on the frequency of the laser pulses was formulated.

2. Experimental

A scheme of the experimental setup for LDG [6] is shown in Fig. 1. The setup consists of a Nd:YAG pulsed laser with a custom designed optical system which was used to shape the laser beam to an annular form. A metal wire is fed vertically and coaxially with the laser beam into its focus. The focus region is flooded with argon shielding gas in order to prevent oxidation.

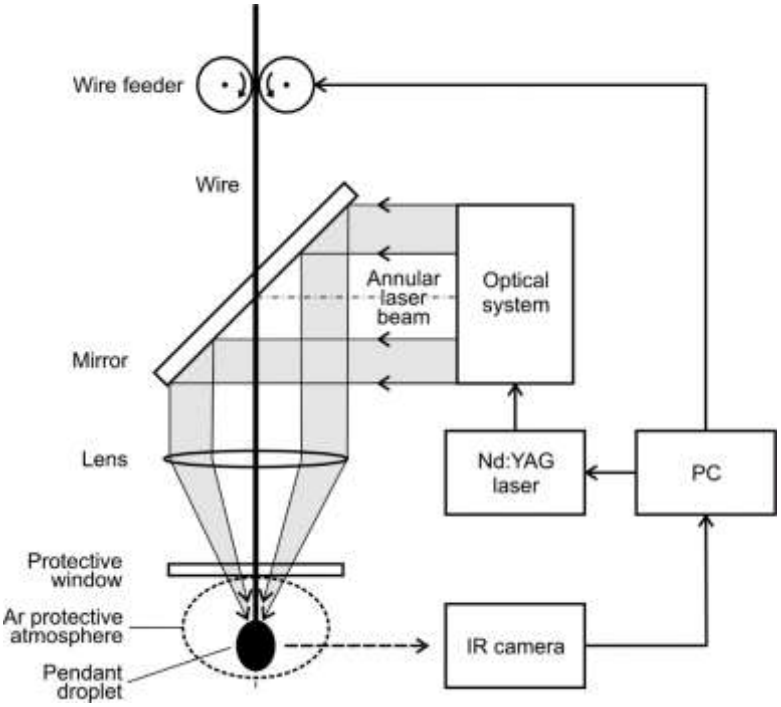

Fig. 1. Scheme of the LDG experimental setup.

In the continuous LDG process, periodic laser pulses are employed in order to melt the wire which is fed into the laser beam focus with a constant velocity. The volume of the pendant

droplet, formed at the wire-end, thus grows steadily due to the inflow of the wire material, melted by the periodic laser pulses, until the droplet is detached. The detachment is either spontaneous due to the action of gravity alone, or additionally stimulated due to the oscillation resonance phenomena of the pendant droplet induced by the laser pulse frequency [5].

The experiments involving continuous LDG were performed with a 0.25 mm diameter nickel wire at constant wire feeding velocity of 0.06 m/s and with rectangular laser pulses of 0.8 ms duration. In order to investigate the influence of the laser pulse frequency f_p on the process, several f_p values between 50 Hz and 300 Hz were selected. In the experiments, the laser pulse power was adjusted to provide the same average laser power of 120 W, which is sufficient to melt the wire, at each of the selected laser pulse frequencies f_p. For the process characterization a high-speed IR sensitive camera was used to capture images of the laser beam focus region. The camera recording frequency was 1445 Hz, with an integration time of 40 μs and an image array size of 64x128.

In Fig. 2 the detached droplet diameter determined from the recorded IR images versus the laser pulse frequency is shown [5]. In this work we focused on the analysis of the so-called mass-spring-like oscillations and the related detachment of the pendant droplet, which took place in the laser pulse frequency f_p range between 60 Hz and 190 Hz, denoted by the black points shown in Fig. 2. We can see that at f_p = 130 Hz, a bifurcation of the droplet diameter d values takes place leading to the simultaneous occurrence of two scattered droplet diameter branches at laser pulse frequencies from f_p = 60 to 120 Hz. In this laser pulse frequency interval, droplets with diameters belonging to both branches were generated in an apparently irregular sequence.

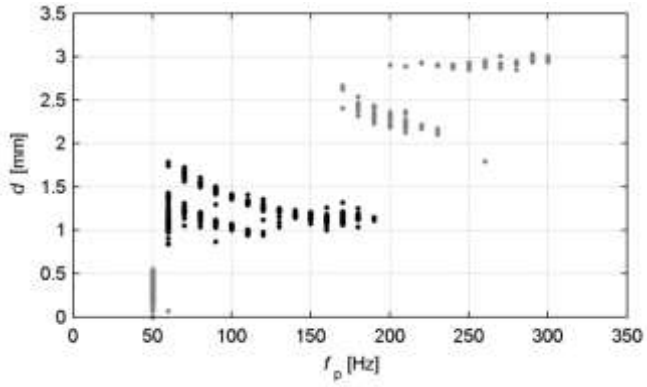

Fig. 2. Experimentally determined detached droplet diameter d as a function of the laser pulse frequency f_p.

An example of a sequence of IR intensity images acquired at f_p = 140 Hz is presented in Fig. 3.In the IR intensity images, the hot droplet with a high IR emission intensity is shown in bright tones, whereas the room temperature background with low IR emission intensity corresponds to the black area. The presented sequence indicates that the observed vertical oscillation of the pendant droplet resembles the oscillation of a mass suspended by a spring. In the time between the two rightmost frames in Fig. 3, the droplet has detached from the solid part of the wire, whose hot end can be seen in the last frame above the detached droplet.

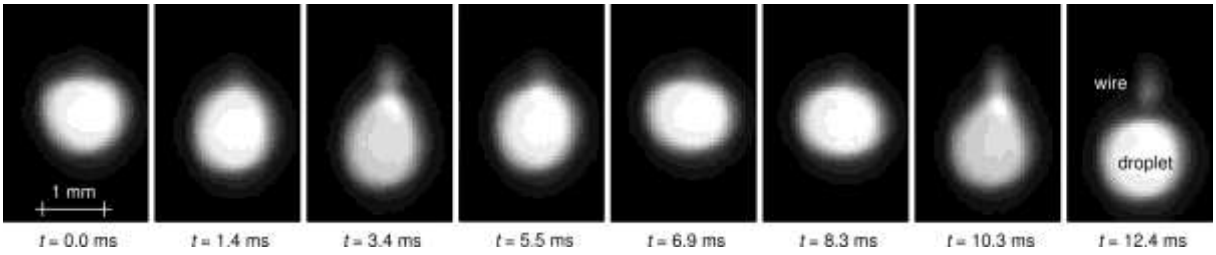

Fig. 3. A sequence of selected IR intensity images showing the vertical oscillation and detachment of the pendant droplet.

In the following, the generation of time series of the droplet centroid's vertical position $y(t)$, the droplet volume $V(t)$, and the IR image maximum value $IR_{max}(t)$ is described. These three time series were then used to characterize the vertical mass-spring-like oscillations and the related mechanism of pendant droplet detachment.

3. Time series generation

The continuous LDG process was characterized by a 30 s long sequence of IR intensity images at each selected laser pulse frequency f_p. Various time series were generated from the recorded image sequences for the purpose of analyzing the influence of the laser pulse frequency f_p on the pendant droplet dynamics. The pendant droplet centroid vertical position time series $y(t)$ and the droplet volume time series $V(t)$ were generated in order to describe and analyze the vertical oscillation of the pendant droplet and the volume of the droplet. Both $y(t)$ and $V(t)$ time series were generated for each detected droplet in the recorded image sequence. Additionally, the IR image maximum value time series $IR_{max}(t)$ was generated for each recorded sequence in order to determine the onset times of the laser pulses, which were

needed to define the phase difference between the droplet vertical oscillation and the laser pulses.

3.1 Droplet centroid vertical position and droplet volume time series

In order to generate the droplet centroid vertical position time series $y(t)$ and the droplet volume time series $V(t)$, the recorded IR intensity images were segmented using the watershed segmentation method on a gradient image [12]. In Fig. 4, an example of segmented images is presented, in which the IR images of Fig. 3 were used as the input. Each segmented image in Fig. 4 includes a background region denoted by a dark grey color and one or more regions denoted by lighter shades of gray, corresponding to the pendant or detached droplets. For example, in the last frame of Fig. 4, a large detached droplet can be seen below a small pendant droplet that has remained on the wire end.

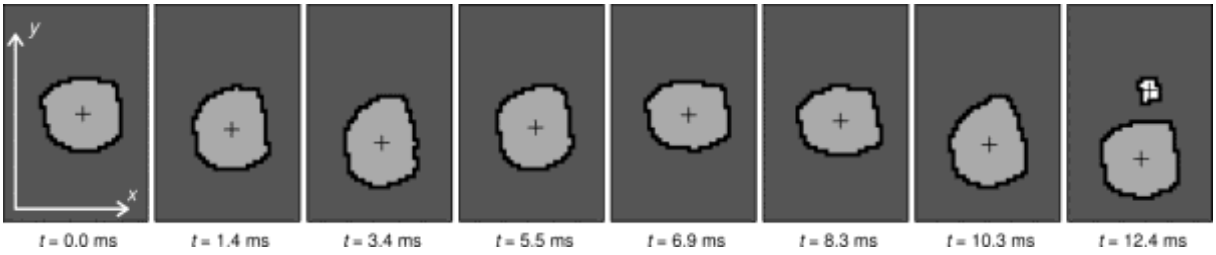

Fig. 4. Example of segmented images with the IR intensity images of Fig. 3 used as input.

Using the droplet regions, determined by image segmentation, the centroid position (x,y) of each droplet was calculated as the center of gravity of the corresponding region with respect to the defined image coordinate system. In Fig. 4, the image coordinate system is shown in the first frame, and the determined droplet centroids are denoted by crosses. The volume V of the droplets was calculated based on the assumption that the identified droplet regions are a central longitudinal cross-sections of axially symmetrical droplets.

For each individual droplet, a corresponding centroid vertical position time series $y(t)$ and a volume time series $V(t)$ were generated by constructing time sequences of the droplet's centroid vertical position y and volume V, respectively, determined from the segmented images. Examples of the resulting time series $y(t)$ and $V(t)$ corresponding to selected values of the laser pulse frequency f_p are presented in Fig. 5.

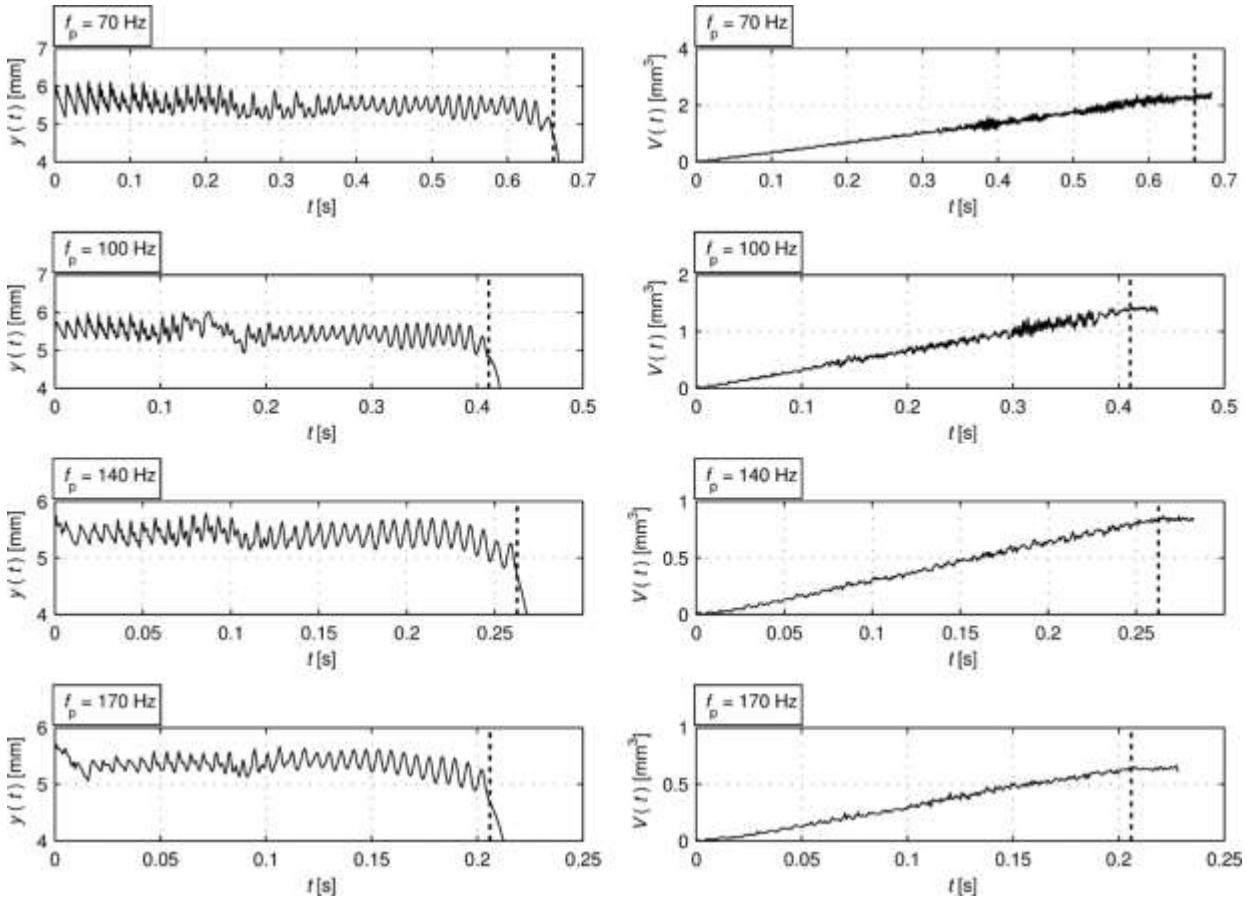

Fig. 5. Examples of the droplet centroid vertical position time series $y(t)$ (left column) and the droplet volume time series $V(t)$ (right column) at selected values of the laser pulse frequency f_p. The dotted vertical line denotes the time t_{det} of the pendant droplet detachment.

The generated droplet centroid vertical position time series $y(t)$ (Fig. 5, left column) exhibits a highly nonlinear and non-stationary oscillation, which was induced by a pulsed laser light melting the wire-end, the formation and growth of the pendant droplet, and the continuous feeding of the wire. In other words, as the laser pulse rapidly melts the wire above the pendant droplet, the melted volume merges with the pendant droplet as the latter is pulled upwards by surface tension. Between the laser pulses, the pendant droplet is pushed downwards with the constant velocity of the wire feed. The upward pulls and the downward movements are rapid and pronounced at the beginning of the LDG process, which is reflected in the saw-shaped initial part of the $y(t)$ time series. Later on, between the upward pulls, the droplet vertical oscillation can be seen superimposed onto a linearly decreasing droplet centroid vertical position, which corresponds to the constant velocity of the wire feed. Due to merging of the melted wire material with the droplet, the droplet volume increases with time, which results both in increasingly smoother oscillation, as well as in decreasing oscillation frequency. For

this reason, in the second half of the $y(t)$ time series, the oscillation becomes smooth with a frequency close to the laser pulse frequency f_p. The abrupt end of the oscillation and the monotonic decrease which can be seen near the end of $y(t)$ time series is caused by the detachment of the pendant droplet, followed by the detached droplet's free fall. In Fig. 5, the time of detachment t_{det} is denoted by a dotted vertical line.

The droplet volume time series $V(t)$ (Fig. 5, right column) increases monotonically as the laser light melts the wire, which was fed with constant velocity. In the initial part of the $V(t)$ time series, step-wise increases in the droplet volume can be observed. They are caused by the merging of the melted wire material with the droplet during each laser pulse. With increasing volume of the pendant droplet, the latter's growth becomes smoother as the large pendant droplet contains enough energy to melt the wire by itself between the laser pulses, and also because the relative increase in the volume decreases and is overcome by the numerical noise. At some parts of the $V(t)$ time series, an increased noise amplitude can be observed. This is the consequence of the excited surface oscillation modes of the pendant droplet [13], which are reflected in the oscillation of the droplet region outline. The monotonic increase of the $V(t)$ time series is disrupted at the time of droplet detachment t_{det}, which is denoted by a dotted vertical line in Fig. 5. After detachment the droplet stops growing, so that after t_{det} the $V(t)$ time series remains constant.

3.2 IR image maximum value time series

In order to define the phase difference between the droplet's vertical oscillation and the laser pulses, the laser pulse onset times had to be determined from the recorded IR image sequences. The method of determination was based on the rapid rise of the IR emission intensity in the focus region during the laser pulse. To detect such an IR intensity rise, the maximum value time series $IR_{max}(t)$ was generated by taking the maximum pixel value of each image in the recorded IR intensity image sequence. For convenience, the resulting $IR_{max}(t)$ time series was rescaled to the unit interval. Due to the similarity between the $IR_{max}(t)$ time series corresponding to the LDG process at different laser pulse frequencies f_p, only the $IR_{max}(t)$ time series at the laser pulse frequency f_p = 100 Hz is presented as an example in Fig. 6a.

In Fig. 6b, part of the $IR_{max}(t)$ time series is enlarged in order to show its characteristic high- and low-frequency components. The high-frequency component, shown as spikes in Fig. 6b,

corresponds to the rapid IR emission variation which follows the temperature variation of the droplet and the wire due to the laser pulse heating. Each spike in Fig. 6b corresponds to a sudden increase in the temperature during the laser pulse, which is followed by an exponential-like decrease resulting mainly due to diffusion of the absorbed energy into the volume of the droplet and the wire. The low-frequency component of the $IR_{max}(t)$ time series consists of a gradually increasing part followed by a sudden decrease, which reflects the gradual growth of the pendant droplet volume followed by its detachment and departure from the image frame. One period of the low-frequency oscillation in the $IR_{max}(t)$ time series thus corresponds to the generation of one droplet.

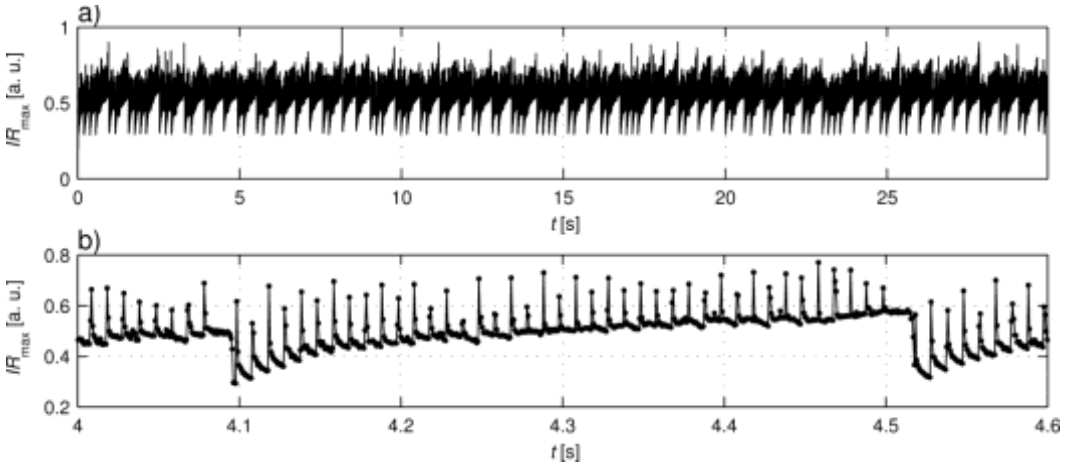

Fig. 6. a) The $IR_{max}(t)$ time series at f_p = 100 Hz. b) Enlarged detail.

4. Time series analysis

In the investigation of the pendant droplet vertical oscillation, the vertical position of the pendant droplet centroid $y(t)$, the volume of the pendant droplet $V(t)$, and the IR image maximum value $IR_{max}(t)$ time series were employed. Due to the non-stationary nature of the pendant droplet centroid vertical position time series $y(t)$ and the experimentally observed presence of resonance phenomena, the $y(t)$ time series were analyzed in the time-frequency domain, using a continuous wavelet transform. The distinct pattern of the $y(t)$ time-frequency representation magnitude, along with the corresponding increasing droplet volume time series $V(t)$, were used to show the mass-spring-like character of the pendant droplet, and to characterize the time-variable mass-spring system by determining its mass and effective spring constant. In order to demonstrate the resonant nature of the droplet detachment, the phase difference between the laser pulses and the pendant droplet vertical oscillation was determined using the $IR_{max}(t)$ time series and the argument of the pendant droplet centroid

vertical position $y(t)$ time-frequency map. Additionally, the detached droplet diameter was predicted depending on the laser pulse frequency f_p, and the predicted values were compared to the experimental ones.

4.1 Time-frequency representation of the droplet vertical oscillation

Time-frequency (*t-f*) analysis is an effective tool for the analysis of transient and nonstationary signals, since it can reveal their time-varying frequency content. Among the various known methods for *t-f* analysis [14], the wavelet transform was chosen for the analysis of the droplet centroid vertical position time series $y(t)$. As a linear *t-f* representation, the wavelet transform is free from cross term interferences and provides a good compromise between time and frequency resolution. For the basis of the wavelet transform, a harmonic wavelet [15] was employed due to its flexibility in selecting the time and frequency resolution, and due to its fast numerical calculation algorithm. In order to improve localization in the time domain, the box-car frequency spectrum of the harmonic wavelet was smoothed, and to improve the *t-f* representation definition, the spectra of adjacent wavelet levels were overlapped [16]. Further, the frequency bandwidth Δf of the harmonic wavelet was chosen to be equal to the center frequency f of the wavelet, which resulted in a duration of the wavelet of the order of $1/f$ [17]. Thus, the corresponding time and frequency resolutions were of the order of $1/f$ and f, respectively.

The *t-f* representation of the droplet vertical position time series $y(t)$ is a complex *t-f* map $Y(t,f)$ with a magnitude $|Y(t,f)|$ representing the amplitude of oscillation and an argument $\arg\big(Y(t,f)\big)$ describing the phase of oscillation. The *t-f* map magnitudes $|Y(t,f)|$ of the droplet centroid vertical position $y(t)$ time series shown in Fig. 5 are presented in Fig. 7 as shaded contour plots. The shading denotes the large values in white and the small values in black, whereas the ten contour levels were selected equidistantly between A - 3σ and A + 3σ, where A is the arithmetic mean and σ is the standard deviation of the corresponding *t-f* map magnitude $|Y(t,f)|$. The large values of the magnitude $|Y(t,f)|$ at the left and right plot edges in Fig. 7 are the results of the wavelet transform edge-effects.

All the generated *t-f* map magnitudes $|Y(t,f)|$ showed a distinct sequence of local maxima $|Y|_{\max,\,i}$ which are marked by white crosses in Fig. 7. The frequencies f_i of the maxima $|Y|_{\max,\,i}$ correspond to multiples of the laser pulse frequency f_p, $f_i = i \cdot f_p$, where $i = 1,2,3\ldots$

This suggests that the maxima are caused by resonance of the droplet vertical oscillation resulting from the impulse-like excitation due to the short laser pulses. In all the presented cases, the last observed maximum occurs only a few laser pulse periods before the pendant droplet detachment, and its frequency equals the frequency of the laser pulses f_p. This further indicates that the detachment is initiated by resonance at $f = f_p$ with accompanying large amplitudes of pendant droplet vertical oscillation.

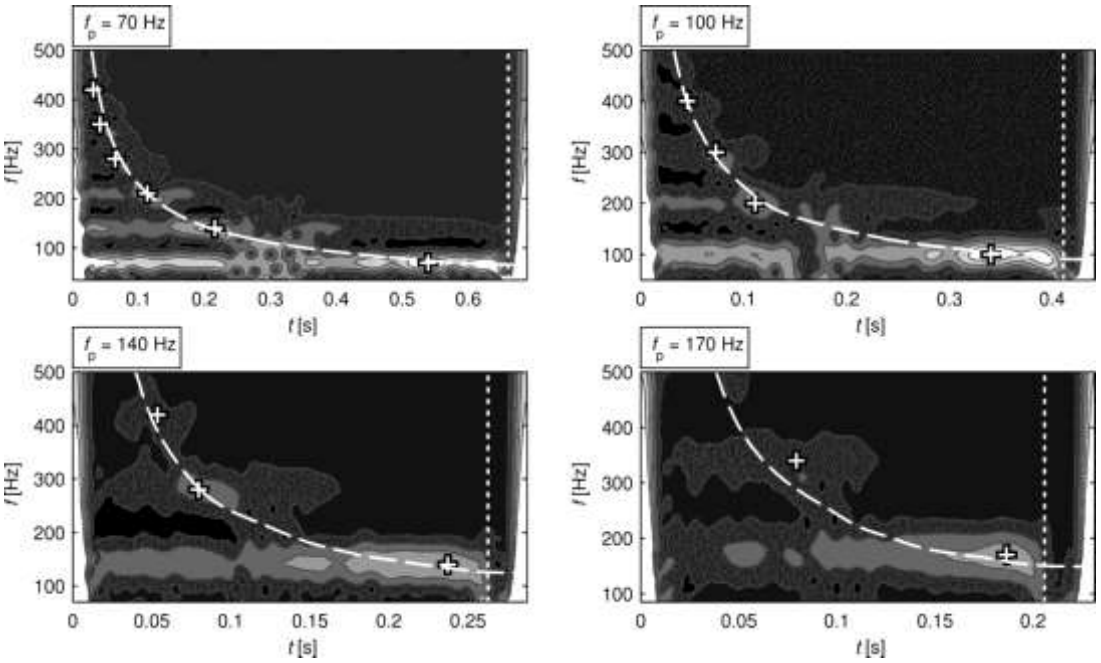

Fig. 7. Shaded contour plots of the *t-f* map magnitudes $|Y(t,f)|$ of the droplet centroid vertical position time series $y(t)$. The white crosses denote the local maxima of the magnitude $|Y(t,f)|$. The white dashed curves correspond to the time-dependent natural frequency $f_d(t)$ of the defined mass-spring system, whereas the droplet detachment time t_{det} is denoted by a dotted vertical line.

4.2 Description of the pendant droplet as a time-variable mass-spring system

The dynamics of a pendant droplet in a continuous LDG process are very complex, since beside the time-dependent droplet volume the process also includes a variety of physical phenomena such as laser light-metal interaction, heat diffusion, phase transitions, surface tension, and fluid flow. As a consequence, an ab initio model of the pendant droplet dynamics would be a high-dimensional one and, therefore, very difficult to define and solve. However, a nonlinear analysis of sequential LDG showed that the dynamics of the LDG process can be modelled by a low, less than five-dimensional dynamic system [11]. For this reason, and

based on the results of the experimental observations, a simple time-variable mass-spring system was selected in an attempt to describe the observed pendant droplet vertical oscillations and gain an analytical insight into the continuous LDG process.

The selection of a mass-spring system was based on the results of visual observation of the droplet oscillation in the recorded IR intensity image sequences, where a distinct vertical oscillation of the pendant droplet could be observed (see Fig. 3), resembling the oscillation of a mass suspended by a spring. The results of the visual observation were supported by the time dependence of the sequence of frequencies f_i of the local maxima $|Y|_{\max,\, i}$, observed in the *t*-*f* map magnitude $|Y(t,f)|$ in Fig. 7. In particular, the time dependence of the frequency sequence f_i corresponded quite well to the time dependence of the natural frequency f_{ms} of a mass-spring system with a linearly increasing mass $m(t)$:

$$f_{\mathrm{ms}}(t) = \frac{1}{2\pi}\sqrt{\frac{k}{m(t)}}, \tag{1}$$

where mass $m(t)$ corresponds to the observed linearly increasing pendant droplet volume $V(t)$ (see Fig. 5 – right column), and k to the corresponding spring constant.

In order to define the mass-spring system corresponding to the pendant droplet, its mass m, its spring constant k, and the viscous damping ratio δ had to be determined. The mass m and the spring constant k were determined from the experimental data, as described below. On the other hand the damping ratio δ could not be experimentally determined due to the laser pulses which periodically interrupted the damped oscillation of the pendant droplet. The length of the uninterrupted damped oscillation was thus limited to at most one laser pulse period $1/f_{\mathrm{p}}$, which, in the most favorable case, corresponds to only a few periods of the pendant droplet oscillation. If, for the sake of acquiring a longer damped oscillation signal, the laser pulses were to be switched off for a certain time, the pendant droplet would start to solidify due to heat conduction into the wire, which would lead to a significant change in the droplet dynamics and a distorted damping ratio δ value. Nevertheless, the damping ratio δ of the pendent droplet was estimated indirectly by setting the damping of the proposed mass-spring numerical model to yield a match between the model results and the experimental data [18]. The resulting estimated damping ratio δ was of the order of 10^{-1}, which means that the relative

difference between the undamped and damped resonant frequencies of the mass-spring system would be of the order of 10^{-2}. Due to the relatively small effect of damping on the resonant frequency, the mass-spring system in this analysis was treated as being undamped.

The time dependent droplet mass $m(t)$ was determined using the droplet volume time series $V(t)$:

$$m_{\mathrm{d}}(t) = \rho\, V(t), \tag{2}$$

where ρ = 7905 kg/m^3 is the density of liquid nickel at the temperature of melting [19]. The effective spring constant k_{d} of the pendant droplet was calculated by combining Eqs. (1) and (2). For each frequency $f_i = i \cdot f_{\mathrm{p}}$ of the experimentally detected local maxima $|Y|_{\mathrm{max},\,i} = |Y(t_i, f_i)|$, occuring at time t_i, the effective spring constant $k_{\mathrm{d}i}$ was calculated from the expression:

$$k_{\mathrm{d}i} = 4\pi^2 f_i^2 \rho\, V(t_i). \tag{3}$$

The droplet volume $V(t_{\mathrm{i}})$ was determined from the pendant droplet volume time series $V(t)$ by taking its value at $t = t_{\mathrm{i}}$.

The above described calculation of the effective spring constant k_{d} was carried out for all the detected *t-f* magnitude maxima $|Y|_{\mathrm{max},\,i}$ for each of the several thousand droplets identified in the recorded image sequences. In Fig. 8, the resulting values of k_{d} are plotted as crosses against the pendant droplet volume V.

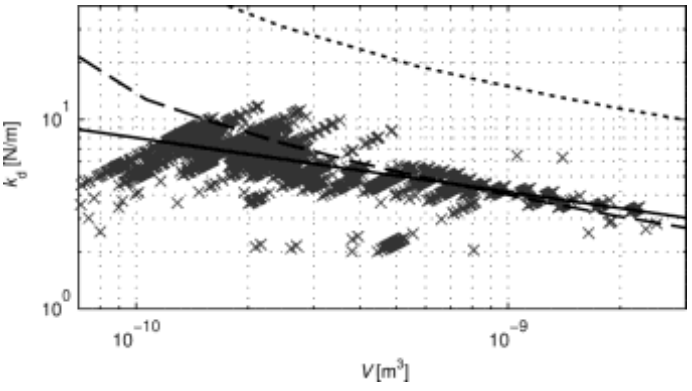

Fig. 8. Calculated values of the pendant droplet effective spring constant k_d plotted against the pendant droplet volume V in a log-log scatter diagram. The full line denotes the power law fit (Eq. (4)). The dotted and dashed curves represent theoretical estimates of the pendant droplet spring constant.

In the log-log scatter diagram shown in Fig. 8, a weak dependence of the effective pendant droplet spring constant k_d on the pendant droplet volume V can be observed. A power law for $k_{pl}(V)$:

$$k_{\mathrm{pl}}(V) = k_0 \cdot \left(\frac{V}{V_0}\right)^a , \tag{4}$$

presented in Fig. 8 by a full line was fitted to the calculated k_d values. The resulting values of the constants were $k_0 = 0.011$ N/m and $a = -0.29$ with $V_0 = 1$ m^3.

Using the power law (Eq. (4)), the time dependence of the natural frequency $f_d(t)$ of the pendant droplet mass-spring system was calculated from the expression:

$$f_{\mathrm{d}}(t) = \frac{1}{2\pi}\sqrt{\frac{k_{\mathrm{pl}}(V(t))}{m_{\mathrm{d}}(t)}}. \tag{5}$$

The function $f_d(t)$ is denoted in the *t-f* map magnitude plots in Fig. 7 as white dashed curves. In Fig. 7, good agreement between the natural frequency time dependence $f_d(t)$ of the calculated mass-spring system and the observed *t-f* map magnitude maxima, marked by white crosses, can be seen.

In order to further support the mass-spring analogy of the observed pendant droplet system, the effective spring constant of the pendant droplet was also estimated theoretically by considering the equilibrium shape of the pendant droplet [20]. To determine the equilibrium droplet shape, the surface tension value of 1.778 N/m [19] corresponding to liquid nickel at its melting temperature was used. A theoretical effective spring constant k_t was estimated from the vertical displacement Δy of the droplet centroid equilibrium position corresponding to the change Δg of the gravity acceleration g_0:

$$k_{\mathrm{t}} = \frac{\Delta F_{\mathrm{g}}}{\Delta y} = \frac{\rho V \Delta g}{\Delta y}. \tag{6}$$

Here, ρ is the density of the liquid nickel at its melting temperature and V is the volume of the droplet. The change Δg in the gravity acceleration g_0 used in the calculation was $\Delta g = \pm 0.1 \cdot g_0$ with $g_0 = 9.81$ m/s^2.

The theoretically estimated effective spring constant k_t of the pendant droplet as a function of the droplet volume V is presented in Fig. 8 by means of a dotted curve. Whereas the slope of this curve corresponds well with the modeled power law (Eq. 4), its values are more than three times larger compared to the experimental values. A similar discrepancy has been previously observed, i.e. in a mass-spring model of a steel pendant droplet [21]. In this case it was attributed to the internal fluid flow of the droplet. It was reported that a halved value of the surface tension had to be used in the model to match the results of the experiment. Based on the above report, the theoretical spring constant was estimated again using the halved surface tension value. The resulting $k_t(V)$ is presented in Fig. 8 by a dashed curve, which agrees relatively well with the experimental results.

4.3 The resonant nature of droplet detachment

In the *t-f* map magnitude $|Y(t, f)|$ diagrams shown in Fig. 7, the time of pendant droplet detachment is denoted by a dashed vertical line. It can be seen that, in all the presented cases, droplet detachment took place only a few laser pulse periods after the occurrence of the last observed magnitude maximum $|Y|_{\max}$. This indicates that the droplet detachment may have been caused by large amplitudes of the droplet's vertical oscillation. Additionally, the preceding analysis suggests that the *t-f* map magnitude maxima were caused by resonances of the pendant droplet mass-spring system driven by the short laser pulses, since the observed maxima always occurred at multiples of the laser pulse frequency f_p. For this reason the observed droplet detachments may have been triggered by resonant high-amplitude oscillation of the pendant droplet, as confirmed by the analysis which is presented below.

In this analysis, the pendant droplet was viewed as a forced time-variable mass-spring oscillator, driven by short laser pulses with a constant laser pulse frequency f_p. Since the mass of the pendant droplet slowly increases with time, the corresponding natural frequency of the

oscillator decreases and the oscillator undergoes resonance when its decreasing natural frequency approaches the external driving frequency. A transition through a resonance can be identified by a maximum of the oscillation amplitude accompanied by a characteristic change in the phase difference between the oscillation of the system and of the driving oscillation. Described in more detail, when the driving frequency is well below the system's natural frequency, the system and the driving oscillations are in phase with one other, the phase difference being 0, whereas at resonance, the phase difference is $\pi/2$, and when the driving frequency is well above the natural frequency, the phase difference is π. In continuous LDG, the external driving was realized by short impulse-like laser pulses with a duration of 0.8 ms. The driving was non-harmonic and its frequency spectrum included the frequency of the laser pulses f_p as well as its multiples $f_i = i \cdot f_p$; $i = 1,2,3,\ldots$ For this reason the pendant droplet's mass-spring system may have experienced a transition through resonance not only at the fundamental driving frequency f_p but also at its multiples.

In the following the phase difference between the droplet vertical oscillation and the laser pulses is defined. It is based on the value of the *t-f* map argument $\arg\big(Y(t,f)\big)$ determined at the time of the laser pulse onset. For this purpose, the laser pulse onset time values $t_{o,j}$, with $j = 1,2,3,\ldots$ being the number of a pulse in a sequence, had to be first determined. It is then shown that the observed *t-f* map magnitude maxima $|Y|_{\max,\,i}$ were accompanied by a characteristic change in the phase difference between the pendant droplet and the driving oscillations from 0 to π. This shows that the observed maxima $|Y|_{\max,\,i}$ were caused by resonance.

The laser pulse onset time values $t_{o,j}$ were determined based on an analysis of the high-frequency component of the IR image maximum value time series $IR_{max}(t)$, which can be seen as sudden amplitude increases in Fig. 6b, caused by the rapid heating of the wire due to the laser pulses. The laser pulse onset time values $t_{o,j}$ were taken to be equal to the time values of the observed sudden amplitude increases. To enhance their detection, an amplitude difference time series $\Delta IR_{max}(t)$ was generated by subtracting each two successive amplitude values in the IR image maximum value time series $IR_{max}(t)$: $\Delta IR_{max}(t_n) = IR_{max}(t_n) - IR_{max}(t_{n-1})$. The initial value $\Delta IR_{max}(t_0)$ was set to zero. The above process of generating the amplitude difference time series $\Delta IR_{max}(t)$ is in fact a Haar wavelet transform of $IR_{max}(t)$ on the smallest scale, which is a suitable choice for the detection of sudden changes in the signal [22].

In Fig. 9a, the resulting $\Delta IR_{max}(t)$ time series, generated from the $IR_{max}(t)$ time series (see Fig. 6), is presented. The sudden amplitude increases in $IR_{max}(t)$ correspond to distinct local maxima above the almost constant background in $\Delta IR_{max}(t)$, of which an enlarged detail is shown in Fig. 9b. However, some local maxima in $\Delta IR_{max}(t)$ do not result from the laser pulse onset but from noise in the experimental data, and were filtered out based on the known periodicity of the laser pulse onset. The maxima corresponding to the laser pulse onset are denoted by circles in Fig. 9b, and their time values were used as the laser pulse onset time values $t_{o,j}$.

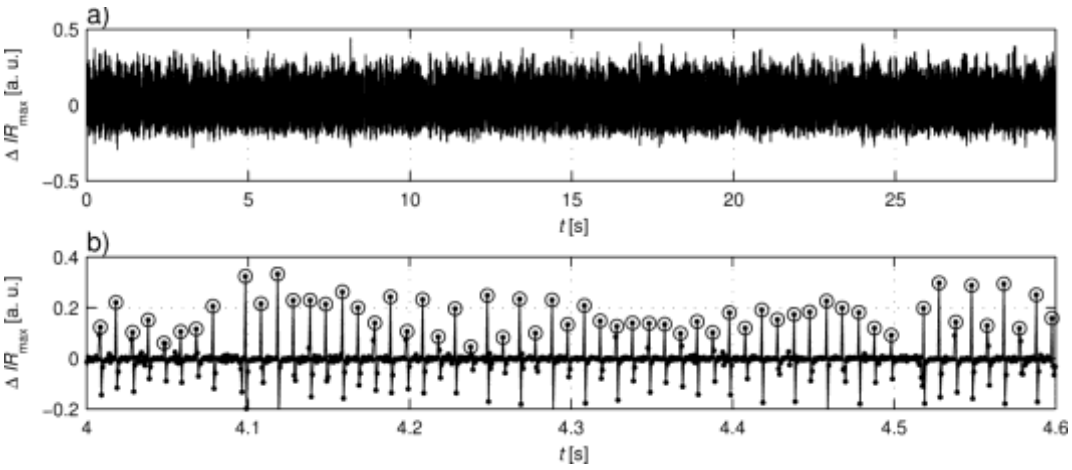

Fig. 9. a) The amplitude difference $\Delta IR_{max}(t)$ time series. b) Enlarged detail. The circles o denote the local maxima, which were used to determine the laser pulse onset time values $t_{o,j}$.

With the determined onset time values $t_{o,j}$, of the laser pulse the phase difference ϕ between the droplet vertical oscillation and the laser pulses was defined based on the argument value $\arg\left(Y\left(t_{o,j}, f\right)\right)$ of the *t*-*f* map at time $t_{o,j}$ of the *j*-th laser pulse onset and at the selected frequency *f*. The pendant droplet vertical oscillation was driven by the melting of the wire above the droplet, caused by the laser pulse, followed by the surface tension force pulling up the droplet. The pendant droplet vertical oscillation was defined to be in phase with the laser pulses ($\phi = 0$) in the case when the oscillating droplet passed the equilibrium position in an upward direction at the moment of the laser pulse onset t_p. It was also assumed that the phase difference ϕ value was positive in the case when the droplet oscillation lagged behind the laser pulses. To comply with the above definitions, the phase difference ϕ between the

droplet vertical oscillation and the laser pulses was defined with the negative value of the *t-f* map argument $\arg\left(Y\left(t_{o,j},f\right)\right)$ and shifted by 3π/2:

$$\phi\left(t_{o,j},f\right)=\frac{3\pi}{2}-\arg\left(Y\left(t_{o,j},f\right)\right). \tag{7}$$

To show the resonant nature of the observed *t-f* map magnitude maxima, the magnitude $|Y(t,f)|$ and the corresponding phase difference $\phi\left(t_{o,j},f\right)$ time dependencies at $f = f_p$ and $f = 2f_p$ are presented in the left and right columns of Fig. 10, respectively, for selected values of the applied laser pulse frequency f_p. Although the maxima of the magnitude $|Y(t,f)|$ and the corresponding characteristic changes of the phase difference $\phi\left(t_{o,j},f\right)$ were also observed at higher multiples of the laser pulse frequency f_p, the lowest two multiples of f_p are shown, where these features are most clearly visible. The large values of the magnitude $|Y|$ near the plot edges in Fig. 10 are a result of the wavelet transform edge-effects, seen also in Fig. 7. The large changes in the phase difference ϕ value after the pendant droplet detachment, indicated by a dotted vertical line in Fig. 10, are the consequence of the phase difference ϕ definition (7), which is not relevant in the case of a detached droplet.

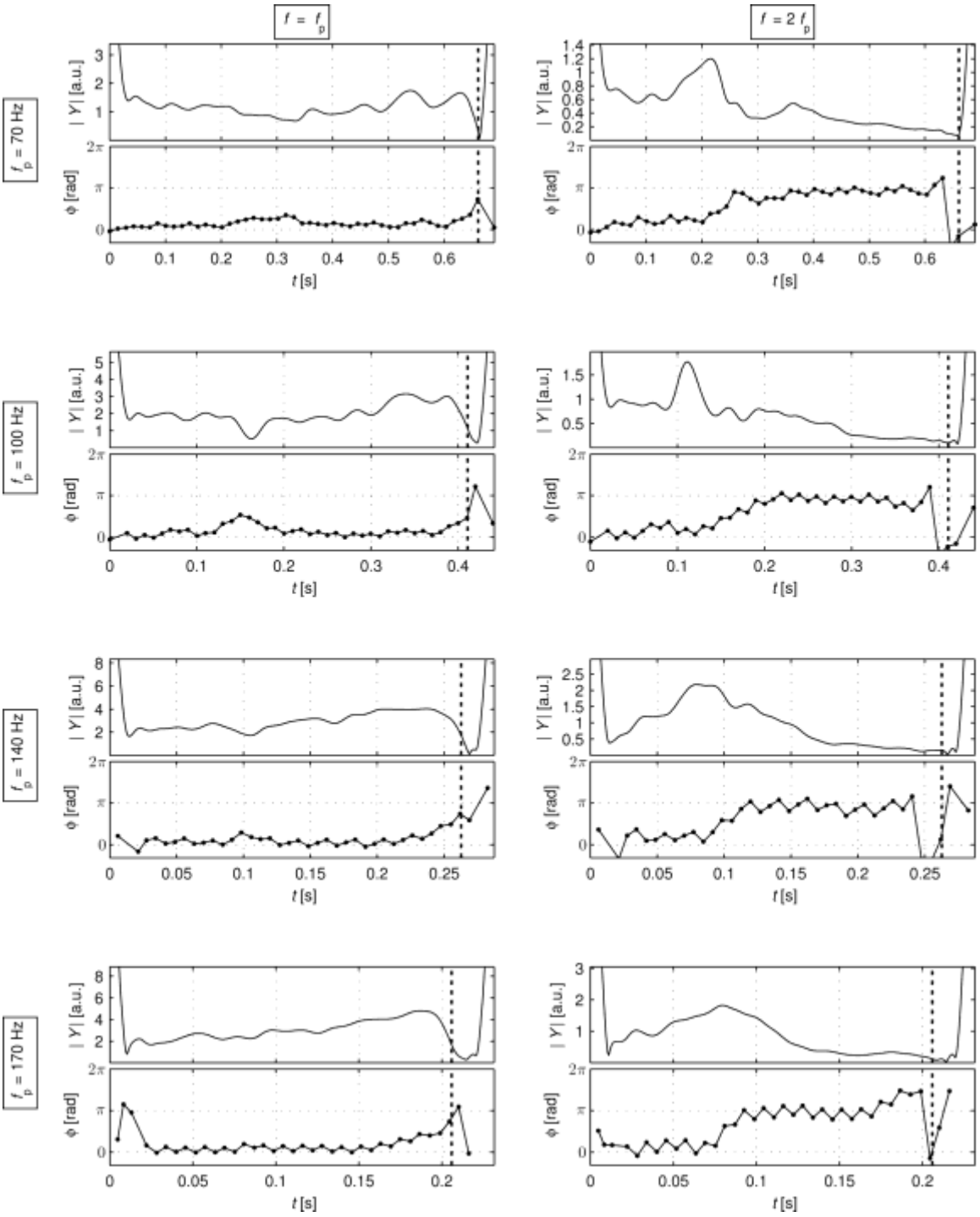

Fig. 10. The *t*-*f* map magnitude $|Y(t,f)|$ and phase difference $\phi(t_{o,j},f)$ time dependencies at $f = f_p$ (left column) and $f = 2f_p$ (right column) for selected values of the laser pulse frequency f_p. The time of droplet detachment is denoted by a dotted vertical line.

In the left column of Fig. 10, the magnitude $|Y(t,f)|$ and phase difference $\phi(t_{o,j},f)$ time profiles at $f = f_p$ are shown. As evident from this figure, maxima of the magnitude $|Y(t,f=f_p)|$, although not very distinct, occur just before the time of pendant droplet

detachment. At the same time, the corresponding phase difference $\phi(t_{o,j}, f = f_\mathrm{p})$, initially near 0, exhibits a rise up to approximately $\phi = \pi/2$ at the time of the pendant droplet detachment. The described behavior was observed at all the selected values of the laser pulse frequency f_p. The magnitude maxima and the related value of the phase difference $\phi = \pi/2$ observed at the moment of detachment show that at detachment the pendant droplet oscillation was in resonance. Being in resonance, the pendant droplet oscillation lagged behind the laser pulses by a quarter period ($\phi = \pi/2$) which means that at the moment of the laser pulse onset, the oscillating pendant droplet was in its low extreme position, i.e. fully stretched. In such a position, the pendant droplet could most easily be detached by Rayleigh-Plateau instability [23] due to the laser beam melting the wire above the droplet. It was therefore concluded that in the observed cases the pendant droplet detachment was caused by resonant vertical oscillation of the pendant droplet, which gave rise to both a large enough oscillation amplitude and an optimal phase difference $\phi = \pi/2$.

In the case of the second multiple of the laser pulse frequency $f = 2f_\mathrm{p}$, shown in the right column of Fig. 10, the magnitude time dependencies $|Y(t, f = 2f_\mathrm{p})|$ exhibit an expressive maximum accompanied by a slightly delayed phase difference change from $\phi = 0$ to $\phi = \pi$. As evident from Fig. 10, both of these occurrences take place well before the pendant droplet detachment, i.e. in the first half of the observed time interval. The maximum and the accompanying change in the phase difference show that the vertical oscillation of the droplet experiences a resonance at the double laser pulse frequency. We can see that the resonance observed at frequency $f = 2f_\mathrm{p}$ occurs sooner than the resonance at frequency $f = f_\mathrm{p}$. This is related to the fact that the former frequency is higher and corresponds to the smaller mass of the growing pendant droplet. In the cases presented in Fig. 10, no pendant droplet detached due to the double laser pulse frequency resonance, presumably because of the too low oscillation amplitude of the smaller pendant droplet mass.

However, in some cases, pendant droplets were also observed to detach at the double laser pulse frequency resonance, which can be attributed to the lateral oscillation of the pendant droplet. Lateral oscillation is also the reason for the above-mentioned not very distinct maxima of the magnitude $|Y(t, f = f_\mathrm{p})|$ (Fig. 10, left column) and the delayed onset of the characteristic change in the phase difference $\phi(t_{o,j}, f = 2f_\mathrm{p})$ (Fig. 10, right column).

The experimentally observed lateral oscillation of the pendant droplet most frequently had a small amplitude, and could have been induced by small asymmetries of the laser beam or of the wire, or their imperfect coaxiality. On the other hand, although rarely observed, lateral instability related large amplitude lateral oscillation may have been excited due to the interaction of the pendant droplet vertical mass-spring-like oscillation and the lateral pendulum-like oscillation modes known as parametric resonance. Such parametric resonance has been predicted and experimentally verified on an elastic pendulum system with a time dependent mass [24]. It is also known that, during the occurrence of such lateral instability, the energy is periodically exchanged back and forth between the vertical and lateral oscillation modes, which influences the amplitudes of both modes.

A qualitative characterization of the experimentally observed parametric resonance and the related phenomena of the unpronounced resonance magnitude $|Y(t,f)|$ maxima and apparently delayed characteristic increase of the phase difference is given in Fig. 11, depicting the vertical position *t-f* map magnitude $|Y(t,f)|$ and the related phase difference $\phi(t_{o,j},f)$ with the corresponding lateral position $x(t)$ of the pendant droplet centroid at the selected $f = f_p$, f_p = 70 Hz (Fig. 11a) and at $f = 2f_p$, f_p = 100 Hz (Fig. 11b). As evident from Fig. 11a, at $f = f_p$, f_p = 70 Hz, the lateral instability is reflected in an onset of lateral oscillation observed in the *x* direction at $t \approx 0.4$ s, which accompanies the resonant maximum in the vertical oscillation magnitude $|Y(t,f)|$. Several alternating increases and decreases of the vertical oscillation magnitude $|Y(t,f)|$ and the amplitude of oscillation in the *x* direction, which are related to the energy exchange cycles between the vertical and lateral oscillation modes, can be seen in Fig 11a. As is also evident, due to the energy exchange, the vertical magnitude $|Y(t,f)|$ maximum is unpronounced. In the case of $f = 2f_p$, f_p = 100 Hz, shown in Fig 11b, lateral instability and a related sudden onset of lateral oscillation in the *x* direction is evident at $t \approx 0.1$ s. Since part of the vertical oscillation mode energy is transferred to the lateral mode, the onset of lateral oscillation is accompanied by a simultaneous decrease in the vertical oscillation magnitude $|Y(t,f)|$. For this reason, in Fig. 11b the characteristic change of phase difference ϕ from $\phi = 0$ to $\phi = \pi$ appears to be delayed with respect to the pendant droplet vertical oscillation magnitude $|Y(t,f)|$ maximum.

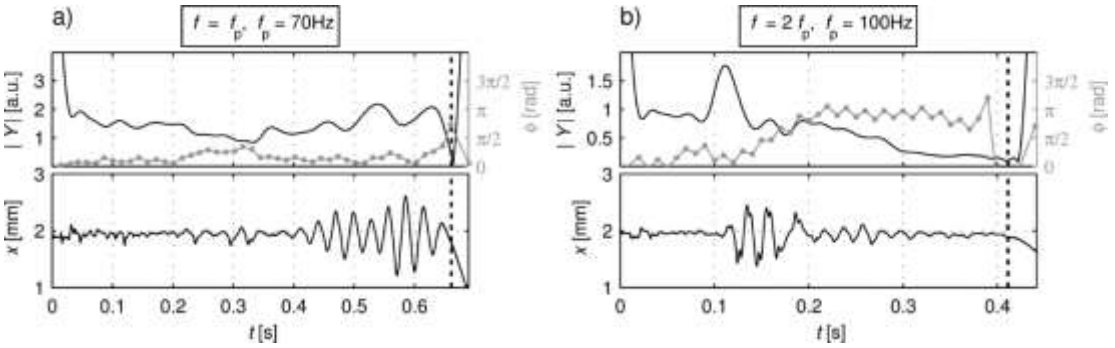

Fig. 11. Examples of experimentally observed pendant droplet lateral instability characterized by the pendant droplet centroid position in the *x* direction, the related vertical oscillation magnitude $|Y(t,f)|$, and the phase difference $\phi(t_{o,j},f)$ at: a) $f = f_p = 70$ Hz and b) $f = 2f_p$, $f_p = 100$ Hz. The time of droplet detachment is marked by a dotted vertical line.

4.4 The generated droplet diameter and its prediction

In view of the droplet characteristics and potential applications, the diameter *d* of a generated droplet is an important process characteristic. Based on the results of the above analysis it can be concluded that in continuous LDG the pendant droplet detachment and the diameter *d* of detached droplets are governed by the frequency f_p of the laser pulses. In more detail, at the end of the fed wire, which is melted by laser pulses, the pendant droplet grows until its natural vertical oscillation frequency, which depends on the pendant droplet diameter, gets into resonance with the laser pulse frequency f_p. The resulting resonant vertical oscillation consequently triggers detachment of the pendant droplet.

In Fig. 12 the experimentally determined detached droplet diameters *d* are shown versus the laser pulse frequency f_p in the interval of the considered frequencies $f_p = [60,190]$ Hz with a step $\Delta f_p = 10$ Hz. The diameter *d* of a detached droplet was estimated from the IR images of the process. It can be seen that droplet diameter *d* is not uniquely defined by the laser pulse frequency f_p, but rather consists of two distinct branches with some experimental scatter of the droplet diameter *d*. Based on the *t-f* analysis of the droplet centroid vertical position time series *y*(*t*) (Fig. 7), it can be established that the upper branch, which spans through the whole interval of the considered laser pulse frequencies f_p, corresponds to droplet detachment due to resonance at frequency $f = f_p$. However, in some cases, at laser pulse frequencies f_p below 130 Hz, the resonant vertical oscillation of the pendant droplet at the double laser pulse frequency $f = 2f_p$ can trigger droplet detachment. Since this resonance frequency corresponds to a lower droplet mass, the resulting observed diameters *d* of the detached droplets are

smaller and constitute the lower branch of the experimental points shown in Fig. 12. In the experiments of the continuous LDG process at $f_p < 130$ Hz both types of resonant detachment coexist and alternate irregularly. The reason for the observed process instability and bifurcation at $f_p = 130$ Hz with the related irregular occurrence of the two detachment types at $f_p < 130$ Hz may be the lateral oscillation of the pendant droplet. As explained above, the lateral oscillation can be excited, either by an uncontrolled asymmetry of the process, e.g. by a small misalignment between the wire axis and the axis of the annular laser beam focus, or by lateral instability due to parametric resonance. If a large enough lateral amplitude is reached it can cause the detachment of droplets of smaller diameter.

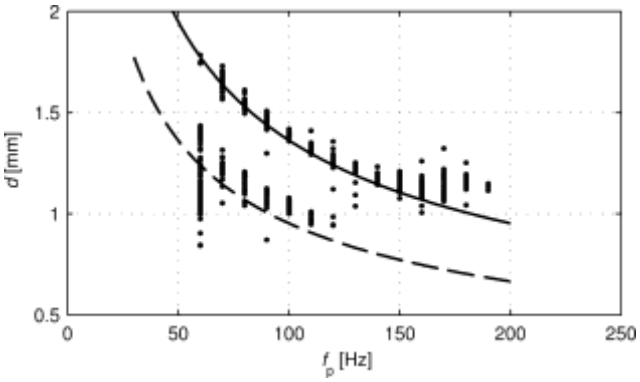

Fig. 12. Detached droplet diameter d as a function of laser pulse frequency f_p: (points) experimental results, (full line) diameter prediction by Eq. (9) with $f_d = f_p$, and (dashed line) diameter prediction with $f_d = 2\ f_p$.

In the following the derivation of an algebraic expression for the prediction of the detached droplet diameter d is presented. The derivation was based on the presented results, which show that in the laser pulse frequency f_p range between 60 Hz and 190 Hz the droplet detachment is triggered by vertical resonant oscillation of the pendant droplet at its natural frequency $f_d = f_p$, and, at $f_p < 130$ Hz, also with $f_d = 2f_p$.

In order to define an expression for the detached droplet diameter $d(f_p)$ dependency on the laser pulse frequency f_p, Eq. (5), which defines the time dependence of the pendant droplet mass-spring system's natural frequency $f_d(t)$, was used. For this purpose, in Eq. (5), the volume V of the approximately spherical droplet and its mass m_d were expressed as functions of the droplet diameter d:

$$V = \frac{\pi d^3}{6},$$

$$m_{\mathrm{d}} = \rho \frac{\pi d^3}{6}. \tag{8}$$

Taking into account the power law expression for the effective spring constant $k_{\mathrm{pl}}(V)$ defined by Eq. 4, the resulting equation was solved for the droplet diameter d

$$d(f_d) = \left(\frac{4\pi^{3-a} \rho V_0^a}{6^{1-a} k_0} \right)^{\frac{1}{3a-3}} f_d^{\frac{2}{3a-3}}. \tag{9}$$

By inserting the values $f_{\mathrm{d}} = f_{\mathrm{p}}$ and $f_{\mathrm{d}} = 2f_{\mathrm{p}}$ for f_{p} = [30, 200] Hz into Eq. (9), the diameters d of droplets detached by resonance at frequencies f_{p} and $2f_{\mathrm{p}}$ were calculated. The resulting diameters d are presented in Fig. 12 by a full and dashed line. It can be seen that the predicted values of detached droplet diameter d follow the general trend of the experimental data of detached droplet diameter d. However, the prediction does not describe the experimentally observed bifurcation near f_{p} = 130 Hz.

5. Conclusions

The pendant droplet vertical oscillation and its detachment in a continuous laser droplet generation (LDG) process were studied based on time series analysis. For this purpose, various time series including the droplet centroid vertical position, the droplet volume, and the IR image maximum values, were generated from the high-speed IR camera records acquired during the LDG process.

The core of the analysis was based on the time-frequency map of the droplet centroid vertical position time series, which was calculated using a continuous wavelet transform employing a harmonic wavelet. Following the observed pattern of the time-frequency map magnitude maxima and the related visual observation of the acquired IR image sequences, the pendant droplet was described as a forced time-variable mass-spring oscillating system. In order to characterize the parameters of the mass-spring system, its mass was determined using the pendant droplet volume time series and its effective spring constant was determined from the positions of the time-frequency map magnitude maxima.

In further analysis, resonant nature of the time-frequency map magnitude maxima was confirmed by observing an accompanying characteristic change of the phase difference between the pendant droplet vertical oscillation and the laser pulses. In order to define the phase difference in addition to the time-frequency map argument, the IR image maximum time series was used. Since in all the observed cases the resonant amplitude maxima of the oscillating droplet occurred directly before detachment, and the phase difference at detachment was $\phi = \pi/2$, it can be concluded that the pendant droplet detachment was triggered by resonance of the pendant droplet oscillation, caused by periodic laser pulses. In the experiments, resonant detachment occurred at the frequency of the laser pulses at all of the investigated laser pulse frequency values. Additionally, at laser pulse frequencies below 130 Hz, resonant detachment at the double laser pulse frequency was also observed, occurring seemingly irregularly. The reason for this irregularity may be a small asymmetry of the experimental setup, giving rise to parametric resonance phenomena and related lateral instability, whose presence was indicated in some of the experimental cases.

The performed analysis showed that the detached droplet diameter depends directly on the laser pulse frequency. Using a forced time-variable mass-spring system description, an algebraic expression of detached droplet diameter dependency on the laser pulse frequency for both observed types of resonant detachment was defined. The defined expression can be used to define an appropriate value of the laser pulse frequency in order to generate a droplet with a pre-defined diameter.

Acknowledgments

This work was supported by ARRS – the Slovenian Research Agency research program P2-0241 and by the COST Action MP1106.

References

[1] E.L. Dreizin, Droplet welding, a new technique for welding electrical contacts, Weld. J. (April 1997) 67-73.

[2] E. Govekar, A. Jerič, M. Weigl, M. Schmidt, Laser droplet generation: Application to droplet joining, CIRP Ann.-Manuf. Techn. 58 (2009) 205-208.

[3] C. Held, U. Quentin, J. Heberle, F. Gürtler, M. Weigl, M. Schmidt, Laser droplet brazing for the electrical contacting of composite materials with integrated active elements, Phys. Proc. 39 (2012) 585-593.

[4] L. Qi, Y. Chao, J. Luo, J. Zhou, X. Hou, H. Li, A novel selection method of scanning step for fabricating metal components based on micro-droplet deposition manufacture, Int. J. Mach. Tool. Manuf. 56 (2012) 50-58.
[5] A. Kuznetsov, A. Jeromen & E. Govekar, Droplet detachment regimes in annular laser beam droplet generation from a metal wire, CIRP Ann.-Manuf. Techn. 63 (2014) 225-228.
[6] E. Govekar, A. Kuznetsov, A. Jerič, Drop on demand generation from a metal wire by means of an annular laser beam, J. Mater. Process. Tech. 227 (2016) 59-70.
[7] E. Govekar, J. Klemenčič, T. Kokalj, B. Jahrsdörfer, P. Mužič, I. Grabec, Characterisation of a laser droplet formation process by acoustic emission, Ultrasonics 42 (2004) 99-103.
[8] J. Klemenčič, T. Kokalj, P. Mužič, I. Grabec, E. Govekar, Characterization of laser droplet formation by reflected light, Opt. Laser Eng. 44 (2006) 398-410.
[9] B. Krese, M. Perc, E. Govekar, The dynamics of laser droplet generation, Chaos 20 (2010) 013129/1-7.
[10] B. Krese, E. Govekar, Nonlinear analysis of laser droplet generation by means of 0–1 test for chaos, Nonlinear Dynam. 67 (2011) 2101-2109.
[11] B. Krese, M. Perc, E. Govekar, Experimental observation of a chaos-to-chaos transition in laser droplet generation, Int. J. Bifurcat. Chaos 21 (2011) 1689-1699.
[12] F. Meyer, Topographic distance and watershed lines, Signal Process. 38 (1994) 113-125.
[13] J. Vejrazka, L. Vobecka, J. Tihon, Linear oscillations of a supported bubble or drop, Phys. Fluids, 25 (2013) 062102/1-18.
[14] Z. Feng, M. Liang, F. Chu, Recent advances in time–frequency analysis methods for machinery fault diagnosis: A review with application examples, Mech. Syst. Signal Proc. 38 (2013) 165-205.
[15] D.E. Newland, Harmonic wavelet analysis, Proc. R. Soc. Lond. A 443 (1993) 203-225.
[16] D.E. Newland, Harmonic wavelets in vibrations and acoustics, Phil. Trans. R. Soc. Lond. A 357 (1999) 2607-2625.
[17] D.E. Newland, Ridge and phase identification in the frequency analysis of transient signals by harmonic wavelets, J. Vib. Acoust. 121 (1999) 149-155.
[18] A. Jeromen, E. Govekar, Modelling of resonant droplet detachment in laser metal droplet generation, Physics Procedia 39 (2012) 863-871.
[19] H. Liu, Science and engineering of droplets: fundamentals and applications, Noyes Publications, Norwich, 2000.
[20] V.A. Nemchinsky, Size and shape of the liquid droplet at the molten tip of an arc electrode, J. Phys. D. Appl. Phys. 27 (1994) 1433-1442.

[21] L.A. Jones, T.W. Eagar, J.H. Lang, A dynamic model of drops detaching from a gas metal arc welding electrode, J. Phys. D Appl. Phys. 31 (1998) 107-123.
[22] E.L. Schukin, R.U. Zamaraev, L.I. Schukin, The optimisation of wavelet transform for the impulse analysis in vibration signals, Mech. Syst. Signal Proc. 18 (2004) 1315-1333.
[23] J.A.F. Plateau, Experimental and theoretical statics of liquids subject only to molecular forces, Gauthier-Villars, Paris, 1873.
[24] N. Danilović, M. Kovačević, V. Babović, Could a variable mass oscillator exhibit the lateral instability?, Kragujevac J. Sci. 30 (2008) 31-44.